FULL PAPER

Near-Field Enhanced Plasmonic-Magnetic Bifunctional Nanotubes for Single Cell Bioanalysis

Xiaobin Xu, Huifeng Li, Dihan Hasan, Rodney S. Ruoff, Alan X. Wang, and D. L. Fan*

Near-field enhanced bifunctional plasmonic-magnetic (PM) nanostructures consisting of silica nanotubes with embedded solid nanomagnets and uniformly dual-surface-coated plasmonic Ag nanoparticles (NPs) are rationally synthesized. The solid embedded sections of nanotubes provide single-molecule sensitivity with an enhancement factor up to 7.2×10^9 for surface-enhanced Raman scattering (SERS). More than $2\times$ SERS enhancement is observed from the hollow section compared to the solid section of the same nanotube. The substantial SERS enhancement on the hollow section is attributed to the dual-sided coating of Ag NPs as well as the near-field optical coupling of Ag NPs across the nanotube walls. Experimentation and modeling are carried out to understand the dependence of SERS enhancement on the NP sizes, junctions, and the near field effects. By tuning the aspect ratio of the embedded nanomagnets, the magnetic anisotropy of nanotubes can be readily controlled to be parallel or vertical to the long directions for nano-manipulation. Leveraging the bifunctionality, a nanotube is magnetically maneuvered to a single living mammalian cell amidst many and its membrane composition is analyzed via SERS spectroscopy.

1. Introduction

Bifunctional plasmonic-magnetic nanoparticles (PM-NPs) are unique hybrid nanomaterials consisting of both optical and magnetic components in a rationally designed nanoscale architecture and have recently attracted intense research interest.[1] Possessing both enhanced optical and magnetic properties, PM-NPs can be extremely useful for biomedical applications that require either optical sensing/imaging/heating, magnetic stimulation/manipulation, or both functionalities.[1a,b,d,2] For instance, PM-NPs can attach to biological entities such as cells and molecules to separate those entities under external magnetic fields and simultaneously detect their chemical nature via optical sensing.[3] The PM-NPs can also be deployed to study the mechanical properties of deeply embedded biological tissues by magnetic field-induced mechanical stimulation[4] and monitoring the responses by in-situ optical imaging.[5] However, current available bifunctional PM nanostructures have been largely limited to quasi-zero–dimensional (0D) nanostructures, such as nanospheres and nanoshells.[1a–d,2a] To our knowledge, there are few reports on quasi-one-dimensional (1D) PM nanostructures, although 1D PM nanostructures provide exclusive advantages for biomedical applications that are unavailable for 0D nanostructures.

In this report, we present a unique type of 1D PM nanotubes and demonstrate their application in targeted single-cell sensing. The PM nanotubes consist of silica nanotubes with embedded solid Ni nanomagnets and uniformly dual-surface-distributed plasmonic Ag NPs. The PM nanotubes provide a high hotspot density (approximately $1200/\mu m^2$ on the outer surface) at the junctions of Ag NPs for SERS biodetection. The solid embedded sections of nanotubes provide single-molecule sensitivity with an enhancement factor up to 7.2×10^9. More than $2\times$ SERS enhancement was observed from the hollow sections than that from the solid section of the same nanotube. This substantial SERS enhancement is induced by the double sided coating of Ag NPs on the nanotubes as well as the near-field optical coupling between Ag NPs on the inner and outer surfaces of the nanotubes. The dependence of SERS enhancement on the particle sizes, junctions, and the near field effects was carried out by both experimentation and modeling. The magnetic anisotropy of the nanotubes, due to the embedded nanomagnets, can be readily tuned to be parallel or vertical to the long direction of the nanotubes for controlled manipulation. Leveraging the nanotubes' unique bifunctionality, we magnetically maneuvered a nanotube to a living Chinese hamster ovary cell and detected the membrane composition of the specific cell with SERS spectroscopy. These bifunctional nanotubes are desirable for multiple-task applications in single-cell bioanalysis, biochemical detection, imaging-contrast enhancement, magnetic manipulation and separation, and biosubstance delivery.

There are three outstanding features provided by the 1D PM nanotubes: First, the unique longitudinal geometry of nanotubes is compatible with both biological cells and biomolecules in terms of length and diameter. For instance, the lengths of

X. Xu, Dr. H. Li, Prof. R. S. Ruoff, Prof. D. L. Fan
Materials Science and Engineering Program
Texas Materials Institute
Department of Mechanical Engineering
The University of Texas at Austin
Austin, TX 78712, USA
E-mail: dfan@austin.utexas.edu
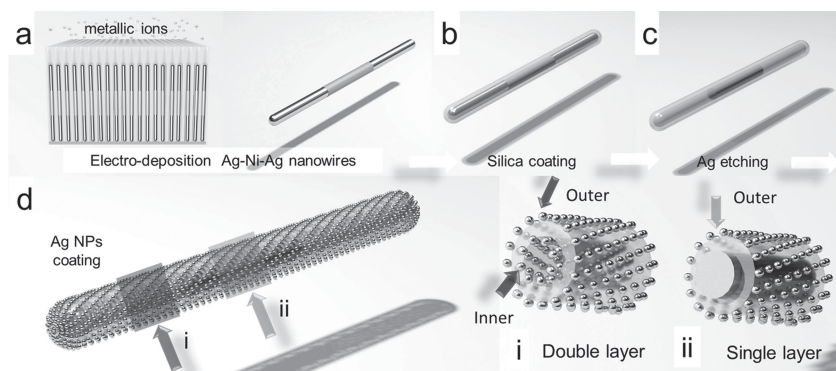D. Hasan, Prof. A. X. Wang
School of Electrical Engineering and Computer Science
Oregon State University
Corvallis, OR 97331, USA

**ADVANCED
FUNCTIONAL
MATERIALS**

www.afm-journal.de

Materials Views

www.MaterialsViews.com

FULL PAPER

Scheme 1. Schematics of fabrication of the PM nanotubes. a) Electrodeposition of Ag/Ni/Ag nanowires. b) Silica shells coating. c) Etching of Ag segment to get hollow nanotubes with solid Ni embedment. d) Synthesis of Ag NPs on both the inner and outer surfaces of nanotubes. Insets are cross-section view of i) the hollow segment and ii) the Ni embedded segment of the PM nanotubes.

nanotubes can be adjusted to tens of micrometers for efficient attachment, manipulation, and separation of cells.[6] The nanoscale diameters restrict the number of molecules that one nanotube can interact with, which is important for molecule-level biosensing and drug delivery.[7] Second, substantially enhanced plasmonic properties are sensitively obtained in the nanotubes. The plasmonic NPs coated on the entire surfaces of the nanotubes provide large and uniform SERS EFs, similar to those frequently reported in patterned substrates,[8] which are provided by traditional 0D plasmonic NPs or their aggregates. Third, by controlling the aspect ratio of the embedded Ni nanosegment, the magnetic moment and anisotropy can be facilely tuned to the desired value, which is important for efficient magnetic separation and manipulation.[9]

2. Results and Discussion

2.1. Design and Fabrication

In order to synthesize such PM nanotubes, a rationally designed four-step approach has been used: 1) multi-segment Ag/Ni/ Ag (3/3/3 µm) nanowires were electrodeposited as growth templates for silica nanotubes (**Scheme 1**a and **Figure 1**a); 2) a layer of silica, with controlled thickness of 70 nm, was uniformly plated on the outer surface of the Ag/Ni/Ag nanowires (Scheme 1b) via hydrolysis of tetraethyl orthosilicate;[10] 3) the Ag segments were selectively etched, resulting in the hollow silica nanotubes with magnetic Ni embedment (Scheme 1c and Figure 1b); 4) plasmonic Ag NPs were uniformly coated through PVP assisted catalysis[11] on the inner and outer surfaces of the nanotubes with optimized particles and junction sizes (Scheme 1d and Figure 1c,e). For detailed fabrication process, see experimental section.

Scanning electron microscopy (SEM) images show that hollow nanotubes with embedded cylindrical solid segments were successfully synthesized (Figure 1c). Energy dispersive X-ray spectroscopy (EDS) confirmed that the cylindrical solid was Ni (Supporting Information Figure S1). By using the same method, multiple Ni nanodisks with controlled

magnetic anisotropies (thickness of 30 nm) can be readily embedded in the nanotubes (to be discussed) (Figure 1d). On the entire outer surface of nanotubes, arrays of Ag NPs were uniformly distributed (Figure 1e). The Ag NPs also grew on the interior surfaces of the nanotubes as shown in the SEM images obtained by cross-sectional focused ion beam (FIB) milling (Figure 1f). The Ag NPs were semi-spherical and densely arranged, yet overlapping NPs were rarely found.

The Ag NP sizes and junctions can be optimized for highly sensitive SERS detection. With fixed volume of nanowire suspension (5.7×10^8/mL, 400 µL) and PVP (10 mL of 2.5×10^{-5} M in ethanol), we systematically varied the total volume of $AgNO_3$ (0.06 M) and $NH_3 \cdot H_2O$ (0.12 M) (v:v 1: 1) from 20 µL to 1200 µL, i.e. 20 µL (0.2× sample), 600 µL (6× sample), 800 µL (8× sample), and 1200 µL (12× sample). The morphologies of the as-synthesized nanotubes showed distinctive particle and junction sizes (Supporting Information Figure S2). The average diameters of the Ag NPs increased from 10.2 ± 2.4 nm (0.2× sample) to 24.8 ± 6.7 nm (8× sample) with the volume of the $AgNO_3$/$NH_3 \cdot H_2O$ solution. The density of Ag NPs reached a maximum in the 6× sample (2050/µm²). The detailed characterization is given in Supporting Information
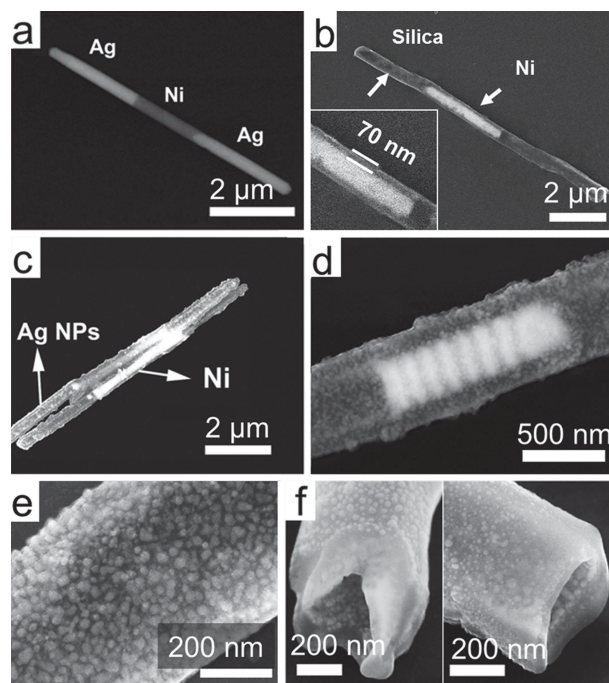

Figure 1. SEM images of a) multisegment Ag/Ni/Ag nanowires, b) silica nanotubes embedded with Ni nanomagnets, c) silica nanotubes with high-aspect-ratio Ni segments and surface-coated Ag NPs, d) low-aspect-ratio Ni segments in the nanotubes, e) close view of the Ag NPs on nanotube surface, and f) cross-sectional images of nanotubes obtained by FIB milling show the nanotubes are hollow with Ag NPs on both the inner and outer surfaces.

Figure S3, S4 and S7. The variation of the particle sizes may be attributed to the dynamic competition between nucleation and crystalline growth of Ag NPs, which has been commonly observed in NP growth.[12]

2.2. SERS Characterization

The SERS performance of the nanotubes were characterized and understood by experimentation and numerical simulation. It is known that a laser-beam focused on two closely neighboring Ag NPs can generate high-intensity electric (E) field in the narrow junction (a few nm) due to localized surface plasmonic resonance as a result of coherent electron oscillation in the Ag NPs. The junction with enhanced E-field is often referred as "hotspot". If a molecule is in the vicinity of a hotspot, its Raman scattering signals can be significantly amplified with $|E|^4$ dependence. This phenomenon is the so-called surface enhanced Raman scattering (SERS).[13] SERS EF is largely determined by E-field intensity and thus the sizes of junctions. If we only consider extremely narrow junctions (<2 nm) on the nanotubes, which contribute most to SERS enhancement, the density of hotspots on the outer surface of nanotubes went up from ≈0/μm^2 for the 0.2× sample to the maximum of 1200/μm^2 for the 8× sample (Supporting Information Figure S6). The corresponding average hotspot sizes can also be determined. The 8× samples provided the smallest average size of hotspots (1.16 nm) and the 6× sample gave the largest (1.4 nm) as shown in **Figure** 2d and Supporting Information Figure S6.

To characterize the SERS performance of nanotubes, we employed standard Raman probes including Rhodamine 6G (R6G) (1 μM to 1 fM) and 1,2-bi-(4-pyridyl) ethylene (BPE) (1 mM). All of the nanotubes can detect R6G and BPE molecules except the 0.2× sample (Figure 2a,e). SERS intensity

increased with the concentration of R6G (Figure 2a,b from the 8× sample). As low as 100 fM R6G can be decisively determined with a signal-to-noise ratio of 7.2 (Figure 2c). The SERS EF values were estimated by following a well-established approach.[14] The highest EF of 7.2×10^9 was obtained from the 8× sample on the Ni embedded sections (Supporting Information Figure S6). According to bianalyte studies, an EF value of above 10^9 is sufficient for single-molecule sensing of various biochemical species.[3,15] The sensitivity of our nanotubes is already on the single molecule levels.

Interestingly, we also noticed that Ag NPs not only grew on the outer surface of the nanotube, but also on the interior surface of the nanotube as shown in the SEM images of cross-sections obtained by focused ion beam (FIB) milling (Figure 1f). Therefore, there were double-layer Ag NPs on the hollow parts of the PM nanotubes and single-layer Ag NPs on the solid part of the nanotubes (Scheme 1 inset). Due to characterization difficulties, we cannot directly measure the size and distribution of the inner layer Ag NPs. However, the effect of the inner surface coating of Ag NPs, can be known from SERS measurement. When a laser beam scanned along a single nanotube with 70 nm thick silica coating, the hollow segments of nanotubes with double-layer Ag NPs exhibited more than two-time SERS intensity than those from single-layer Ag NPs on the outer surface of the Ni embedded section of nanotubes (Figure 2g). Similar results were also observed when we replaced the Ni segment with Pt (Figure 2h). The experimental details are provided in Supporting Information Figure S5.

2.3. Plasmonic Simulation

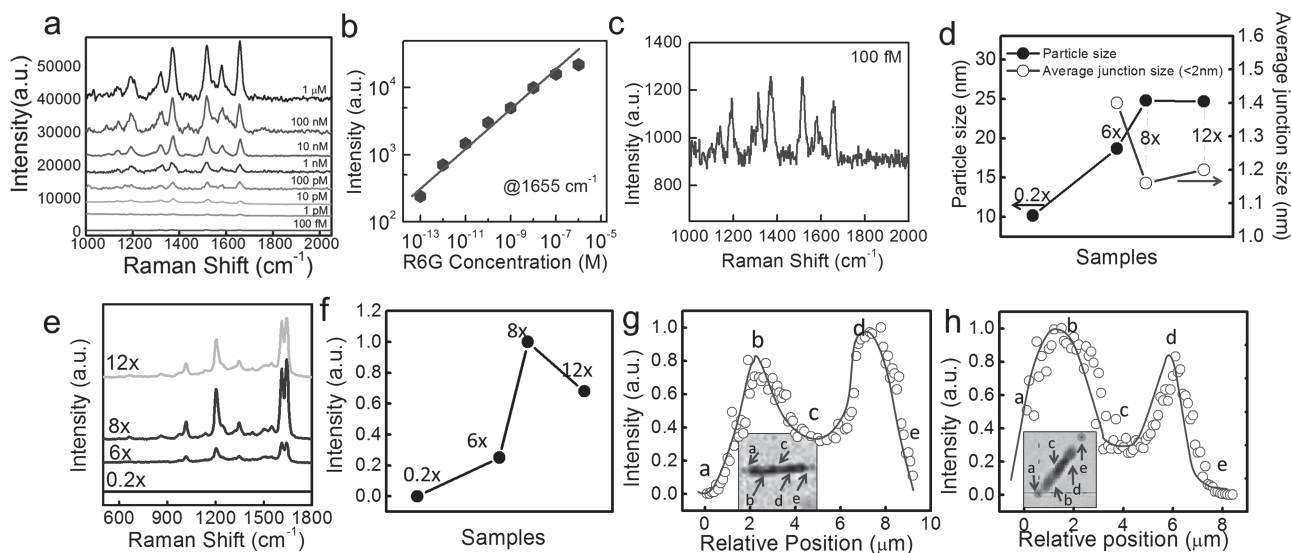It is interesting to understand how the EF depends on Ag particle and junction sizes, as well as how the Ag NPs on the

Figure 2. a) SERS spectra of R6G detected from the 8× nanotube sample from 100 fM to 1 μM, b) SERS intensity at 1655 cm^{-1} increases with the concentration of R6G. c) Concentration as low as 100 fM of R6G was detected from the 8× sample. d) Particle size and average hotspot size (<2 nm) of different samples. e) SERS spectra of 1 mM of BPE taken from nanotubes fabricated at various conditions. f) SERS intensity of nanotubes fabricated at different conditions. SERS intensity scanning along nanotubes with solid embedment in the center: g) Ni embedded and h) Pt embedded hollow nanotubes.
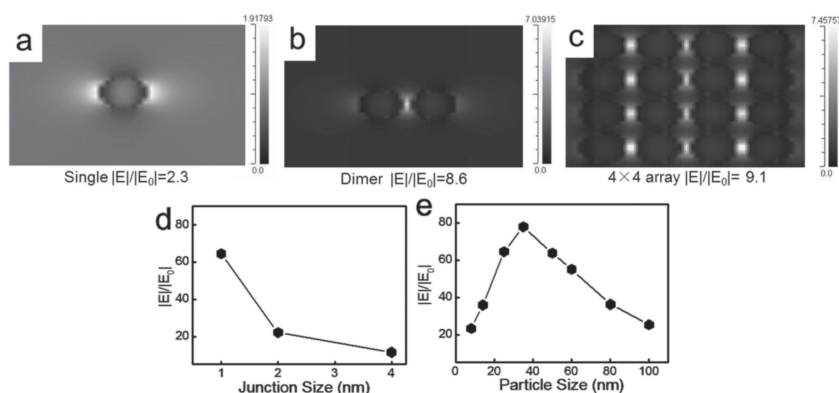
FULL PAPER

Figure 3. Simulation results for Ag NPs of 20 nm in diameter and junction (if any) of 3 nm: a) a single Ag NP; b) a dimer of Ag NPs and c) a 4 × 4 Ag NP array. The *E*-field enhancement is the highest in the 4 × 4 Ag NP array and lowest in a single Ag NP. d) The *E*-field EF increases with decrement of the junctions (with fixed particle size of 25 nm). e) The *E*-field EF reaches the maximum value when the particle size is between 30 and 40 nm with a fixed junction of 1 nm.

hollow structures can further enhance SERS. Numerical simulation was conducted for such a purpose. We only compare the nanotubes that are fabricated in the same batch (300 nm in inner diameter and 70 nm in shell thickness).

It is known that the SERS enhancement can be attributed to two factors: *E*-field enhancement due to the plasmonic resonance of NPs and chemical enhancement due to charge transfer between the molecules and metal particles.[3] The *E*-field enhancement can be approximated as[15b] $EF \approx \frac{|E(\omega_L)|^4}{|E_0|^4}$ where ω_L is the resonant angular velocity of the local field E in an external field of E_0. Due to the quadruple dependence on the local E field, the *E*-field enhancement is usually considered to be a major contributor to SERS. We used a 3D finite difference time domain (FDTD) method to simulate this effect. We simulated the normalized electric field ($|E|/|E_0|$) close to the Ag NPs. The excitation wavelength was set at 532 nm with in-plane polarization perpendicular to the nanotube surface. To find the effect of NP junctions on SERS EF, we began with the simulation for a single particle, a dimer, and then a 4 × 4 array (**Figure 3**a–c, the shape of Ag NPs was assumed to be cylindrical with a uniform thickness of 20 nm. The junction was set at 3 nm). A single silver NP provided electric field enhancement of $|E|/|E_0|$ = 2.3, hence the SERS EF = 28 due to the E^4 dependence; metal dimers and a 4 × 4 array provided $|E|/|E_0|$ = 8.6 (EF_{SERS} = 5470) and $|E|/|E_0|$ = 9.1 (EF_{SERS} = 6857), respectively. This simulation confirms that a group of metallic particles on the same surface can provide stronger E field enhancement than that of single particles or dimers.

A group of NPs with controlled distributions should further enhance the E field. Therefore we simulated the *E*-field enhancement depending on junctions of the particle arrays. As plotted in Figure 3d, narrower junctions between NPs exhibit a strong electric field for an array with Ag NPs of 25 nm in diameter. At a fixed junction of 1 nm, the highest electric field enhancement is obtained in particle arrays with diameters between 20–50 nm as shown in Figure 3e. The simulation results excellently agree with previous work, which refers to such results as proof of the "extrinsic size effect".[16] For NP with larger sizes (>40 nm), the *E*-field enhancement reduces because the plasmonic resonance

shifts to longer wavelength. When such NPs are excited by short-wavelength lasers, they induce higher-order electron cloud distortion of conduction electrons and thus degrade the plasmonic resonance. For NPs that are less than 25 nm, scattering of electrons from the particle's surfaces produces a damping term that is inversely proportional to the particle diameter. This means that more optical energy is converted to heat instead of being scattered to produce local field enhancement. As a result, by comparing the electric fields among NPs with different diameters and junctions, we have optimized the design of the Ag NPs. The result of simulation readily explained our experimental observation: among all the samples, the 8× samples with the largest diameters (24.8 ± 6.7 nm) and smallest gaps (≈1.16 nm) offered the highest SERS EF.

To understand how the dual-side-Ag-coated hollow nanotubes can further enhance SERS than the single-side-Ag-coated nanotubes with solid embedment do, we carried out numerical simulations by Comsol 3.5a RF module. In our modeling, a 3D silica nanotube is constructed (illustrated in Scheme 1d and insets): the inner cylinder radius is 150 nm, and the shell thickness is 70 nm. The densely coated Ag NPs are simplified by a 2D conformal array attached to the outer and inner surfaces of the silica nanotubes. The Ag NP diameter is 25 nm and the gap between them is 2 nm. The silica nanotube is placed on top of a glass substrate, and is excited by a surface normal Gaussian beam with beam diameter of 1 μm at 532 nm wavelength. The polarization direction is perpendicular to the axis of the cylinder. **Table 1** lists our simulation results corresponding to our experimentally measured devices and **Figure 4** shows the cross sectional views of the electric field distribution of the four devices as listed in Table 1.

In Figure 4a, we surprisingly find that the hot-spot with maximum electric field enhancement is actually at the bottom of the nanotube, not at the top. This is because the bottom hot-spot is surrounded by high-index silica; while the other hot-spots have only one side contacted with silica (other side is exposed to low-index air). Additionally, the inter-particle coupling through the NP chain at the outer surface enhances the electric field at the bottom.[17] Comparing Figure 4a,b, we are able to clearly conclude the contribution of inner layer Ag NPs: the presence of inner layer not only adds more hot spots for SERS sensing, but also significantly increase the intensity of

Table 1. Simulation parameters for plasmonic magnetic nanotubes. *D* is the particle size.

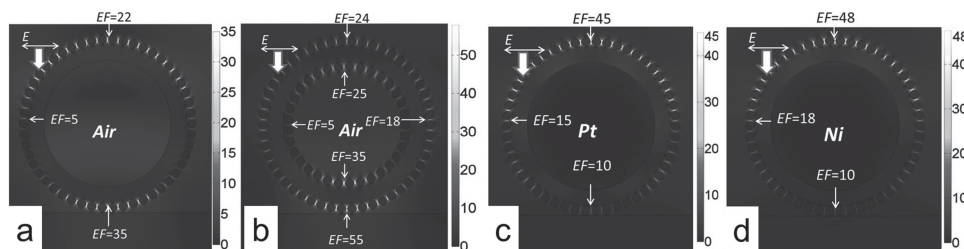|	Outer layer	Inner layer	Ag NPs
Simulation 1	Ag NPs	Hollow (air)	*D* = 25 nm, gap = 2 nm
Simulation 2	Ag NPs	Ag NPs	*D* = 25 nm, gap = 2 nm
Simulation 3	Ag NPs	Pt	*D* = 25 nm, gap = 2 nm
Simulation 4	Ag NPs	Ni	*D* = 25 nm, gap = 2 nm

Figure 4. a–d) Simulation results show the cross sectional views of the optical induced electric field enhancement of the four devices as listed in Table 1.

the hot spots in the outer layer NPs, which is due to the near-field effect[18] of inter-layer coupling between NP chains in the inner and outer surfaces of the nanotubes. When the air core is filled with Pt, which has no surface plasmonic resonance at visible wavelength, we observed interesting phenomena: first, the EF of the hot-spots on top of the nanotube is enhanced roughly 2×, which is due to the reflected light from the Pt core; second, the hot-spots at the bottom of the nanotube, however, is significantly reduced because almost no light can penetrate the Pt core to excite the surface plasmons. And moreover, the inter-particle coupling through the NP chain can be weakened by evanescent field absorption of Pt. Similar electric field enhancement is observed in Ni-filled nanotube as well.

If we assume there are enough molecules so that every hot-spot can contribute to SERS measurement, we can calculate the total SERS signals by $\sum|E_i|_4$, where E_i is the electric field in each hot spot. The total SERS signals of these four devices are 0.8×10^5, 2.5×10^6, 1.4×10^5 and 1.3×10^5 a.u., respectively. It is seen that device 2 will be able to provide more than 10× higher SERS signals than device 3 and 4. However, in reality, the SERS signals from hot-spots at the bottom to the nanotubes are more difficult to collect due to NP scattering. Experimental we obtained more than 2× differences (Figure 2g,h). The comparison of single-side and dual- side Ag NP coated segments in the nanotubes is summarized in Supporting Information Figure S8.
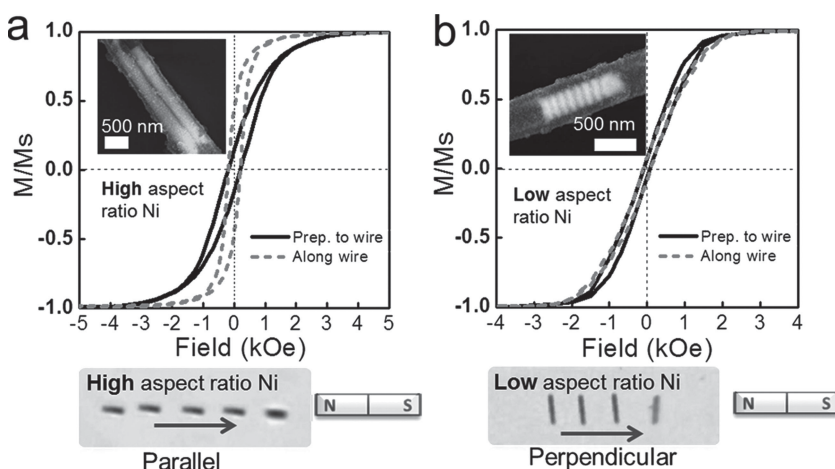
Moreover, we noted that the thickness of silica also affects the enhancement of SERS. We observed near-field enhancement effect on nanotubes with silica coating ranging from 70 to 150 nm. However, when the thickness of silica was increased to 300 nm, the near-field enhancement effect was not observed, which may be attributed to the reduced plasmonic coupling between Ag NPs across the silica shell.

2.4. Magnetic Characterization

Not only plasmonically sensitive, the unique nanotubes also offered tunable magnetic properties for controlled manipulation. The magnetic anisotropy of Ni segment is dominated by its shape anisotropy[9] as opposed to its weak crystalline anisotropy. When the aspect ratio of Ni segment is high, e.g. 10/1 (Ni length 3 um, diameter 300 nm), the anisotropy direction and the easy axis is along the nanotube long axis as measured by vibrating sample magnetometry (VSM) (**Figure 5**a). A hysteresis loop along magnetic easy axis demonstrates higher magnetic remanence and squareness than those measured perpendicular to the nanotubes. When the aspect ratio of the Ni segments is below 1, e.g., a stack of thin Ni disks with diameters of 300 nm and thickness of 30 nm, magnetic anisotropy is generally transverse to the nanotubes with essentially zero remanence due to the anti-parallel coupling of the magnetizations in neighboring nanodisks (Figure 5b). This fascinating way of controlling the magnetic anisotropy has been vividly demonstrated by manipulating nanotubes in suspension with a magnetic field. As shown in Figure 5, nanotubes with magnetic anisotropy along the long axis align with the magnetic field during transport, but those with transverse magnetic anisotropy align perpendicular to the magnetic field. The transport speed was 2–7 μm/s, which can be controlled by the magnetic field gradient.

2.5. Single-Cell Bioanalysis

Although single complex biological samples can be investigated with standard Raman microscopy, a detailed investigation of specific components on the cell surface is not possible with this approach.[19] In our work, we demonstrated the utility of the bifunctional nanotubes in revealing the
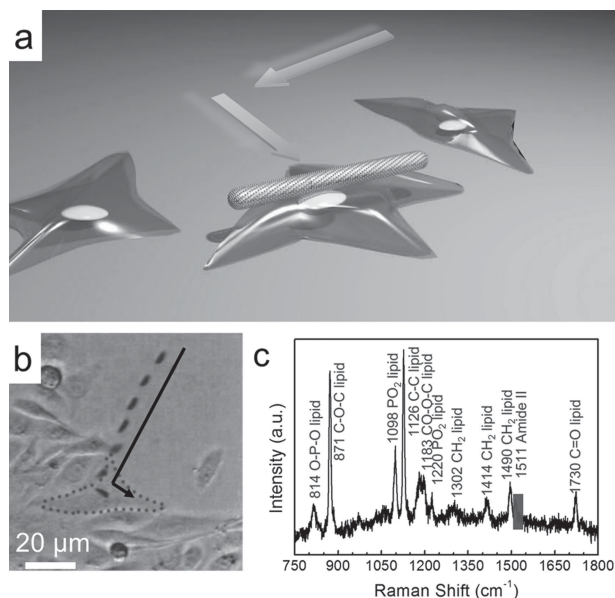

Figure 5. Magnetic anisotropy can be readily tuned by the aspect ratio of magnetic Ni embedment as shown in the hysteresis loops for Ni with a) high and b) low aspect ratios, respectively. The overlapped images show nanotubes transported parallel or perpendicular to the magnetic field due to their unique anisotropies. The speed of nanotubes is 5–7 μm/s.

© 2013 WILEY-VCH Verlag GmbH & Co. KGaA, Weinheim

FULL PAPER

Figure 6. a,b) Transport a nanotube to a single CHO cell amidst many. c) SERS spectrum from the CHO cell membrane is dominated by lipid contribution, and a few peaks can be assigned to protein (blue bar).

membrane composition of a single Chinese hamster ovary (CHO) cell amidst many. We chose CHO cells because they are widely used in biological research, especially in studies of genetics, toxicity screening, gene expression, and expression of recombinan proteins. Here, leveraging the unique bifunctionality of the nanotubes, we can precisely transport a nanotube to a specific living CHO cell (see Experimental Section) amidst many and detected its membrane chemistry with SERS spectroscopy. A PM nanotube was transported and aligned in the direction of the magnetic field and precisely landed on the membrane of a CHO cell (overlapped images in **Figure 6**a,b and Supporting Information Video S9). From SERS spectra (Figure 6c), which was taken from the nanotube with an integration time of 5 s, shows strong characteristic peaks of lipids.[7,19,20] The peak position 1511 cm^{-1} can be assigned to amide II, which is from protein (blue bar in Figure 6c). This results revealed that the cell membrane in contact with the nanotube consists mostly lipids and some protein molecules, which is consistent with real cell membrane composition.[19] Without nanotubes, no Raman signals can be detected from the cell, this clearly demonstrating the highly desirable bifunctionality of the nanotubes for precision and ultrasensitive single-cell bio-analysis. This technique is generally applicable to any adhesive live cells. It can be readily applied to hamster cells as well as to mouse or human cells.

3. Conclusions

In summary, we have successfully designed and synthesized a unique type of near-field enhanced bifunctional PM-active nanostructure that consists of a hosting silica nanotube, a magnetic segment embedded within the nanotube, and Ag

NPs uniformly coated on the dual surfaces of the nanotube. By controlling the fabrication conditions, both the diameter and junction of Ag NPs can be precisely controlled for ultrasensitive molecular sensing. The 3D FDTD simulation of *E*-field enhancement agrees with the experimental results. Higher SERS intensity is found on hollow than the solid parts of the PM nanotubes, and it is confirmed to be from the near field coupling between the inner and outer layer of Ag NPs. The embedded nanomagnets with tunable magnetic anisotropy allow flexible manipulation of the nanotubes with external magnetic fields. Such bifunctional nanostructures can be transported to a living Chinese hamster ovary cell amidst many other cells to reveal the membrane composition. The PM nanotubes are suitable for single-cell bioanalysis as well as various biological applications, such as biochemical sensing, magnetic manipulation, separation, MRI contrast, and biosubstance delivery.

4. Experimental Section

Fabrication of Plasmonic-Magnetic Nanotubes: A series of strategies was implemented to synthesize the unique bifunctional nanotubes using the above approach. In brief, the multisegment Ag/Ni/Ag nanowires were fabricated by electrodeposition in nanoporous anodized aluminum oxide (AAO) templates as reported elsewhere.[11,21] In brief, a Cu layer of about 500 nm in thickness was thermal evaporated onto the back of the template to seal the pores and serve as the working electrode in a three-electrode electrodeposition system. The electrodeposition of metal materials gradually fill the bottom of the nanopores working electrode to form nanowires. Finally, the AAO template was dissolved in 2 M NaOH solution to release the free-standing nanowires. The amount of electric charge passing through the circuit controls the length of nanowires to 7 nm.[22] The pore size of nanoporous template controls the diameters of the nanowires from 20 to 400 nm, with different compositions along the lengths (e.g., Ag/Ni/Ag nanowires) (Figure 1a), and here we prepared 300 nm diameter 3/3/3 μm Ag/Ni/Ag nanowires (−1.1 V for Ag and −1 V for Ni).

Next, the Ag/Ni/Ag nanowires were used as templates for fabricating Ni-embedded silica nanotubes. We first coated an amorphous silica layer on the surface of the Ag/Ni/Ag nanowires. Silica was used due to its porous structure with a high surface area, biocompatible properties, and drug carrier capability.[10a] Here, it also serves as a support substrate for plasmonic Ag NPs. The reaction was accomplished by hydrolysis of tetraethyl orthosilicate for 2–5 h with a controlled thickness of a few to hundreds of nanometers.[10] Next, the Ag segments were selectively etched with a mixture (4:1:1) of methanol (99%), hydrogen peroxide (30%), and ammonia hydroxide (28–30% as NH$_3$), which result in Ni-embedded nanotubes as shown in Figure 1b.

Finally, arrays of plasmonic Ag NPs were uniformly synthesized on the surface of silica nanotubes by reduction of Ag ions with PVP (10 mL, 2.5×10^{-5} M in ethanol) from a mixed solution of silver nitrate (0.06 M, 400 μL) and ammonia hydroxide (0.12 M, 400 μL) at 70 °C for 7 h.

Cell Culture and Reagents: CHO cells (ATCC) were cultured in RPMI medium (Invitrogen) supplemented with 10% fetal bovine serum and 1% penicillin-streptomycin (Invitrogen). Cells were maintained in a humidified 37 °C, 5% CO$_2$ incubator. Before the experiment being conducted, CHO cells were washed by phosphate buffered saline (PBS) followed by addition of nanotubes (dispersed in PBS).

Supporting Information

Supporting Information is available from the Wiley Online Library or from the author.

FULL PAPER

Acknowledgements

[1] a) C. S. Levin, C. Hofmann, T. A. Ali, A. T. Kelly, E. Morosan, P. Nordlander, K. H. Whitmire, N. J. Halas, *ACS Nano* **2009**, *3*, 1379; b) S. Peng, C. H. Lei, Y. Ren, R. E. Cook, Y. G. Sun, *Angew. Chem. Int. Ed.* **2011**, *50*, 3158; c) G. A. Sotiriou, A. M. Hirt, P. Y. Lozach, A. Teleki, F. Krumeich, S. E. Pratsinis, *Chem. Mater.* **2011**, *23*, 1985; d) Z. C. Xu, Y. L. Hou, S. H. Sun, *J. Am. Chem. Soc.* **2007**, *129*, 8698; e) Y. D. Jin, C. X. Jia, S. W. Huang, M. O'Donnell, X. H. Gao, *Nat. Commun.* **2010**, *1*; f) V. V. Temnov, G. Armelles, U. Woggon, D. Guzatov, A. Cebollada, A. Garcia-Martin, J. M. Garcia-Martin, T. Thomay, A. Leitenstorfer, R. Bratschitsch, *Nat. Photonics* **2010**, *4*, 107.

[2] a) Y. T. Lim, M. Y. Cho, J. K. Kim, S. Hwangbo, B. H. Chung, *ChemBioChem* **2007**, *8*, 2204; b) J. H. Gao, G. L. Liang, J. S. Cheung, Y. Pan, Y. Kuang, F. Zhao, B. Zhang, X. X. Zhang, E. X. Wu, B. Xu, *J. Am. Chem. Soc.* **2008**, *130*, 11828; c) N. Insin, J. B. Tracy, H. Lee, J. P. Zimmer, R. M. Westervelt, M. G. Bawendi, *ACS Nano* **2008**, *2*, 197; d) K. C. Weng, C. O. Noble, B. Papahadjopoulos-Sternberg, F. F. Chen, D. C. Drummond, D. B. Kirpotin, D. H. Wang, Y. K. Hom, B. Hann, J. W. Park, *Nano Lett.* **2008**, *8*, 2851; e) C. Xu, J. Xie, D. Ho, C. Wang, N. Kohler, E. G. Walsh, J. R. Morgan, Y. E. Chin, S. Sun, *Angew. Chem. Int. Ed.* **2008**, *47*, 173; f) K. Cheng, S. Peng, C. J. Xu, S. H. Sun, *J. Am. Chem. Soc.* **2009**, *131*, 10637; g) C. J. Xu, B. D. Wang, S. H. Sun, *J. Am. Chem. Soc.* **2009**, *131*, 4216.

[3] X. M. Qian, S. M. Nie, *Chem. Soc. Rev.* **2008**, *37*, 912.

[4] N. J. Sniadecki, C. M. Lamb, Y. Liu, C. S. Chen, D. H. Reich, *Rev. Sci. Instrum.* **2008**, 79.

[5] J. N. Anker, W. P. Hall, O. Lyandres, N. C. Shah, J. Zhao, R. P. Van Duyne, *Nat. Mater.* **2008**, *7*, 442.

[6] a) A. Hultgren, M. Tanase, C. S. Chen, D. H. Reich, *IEEE Trans. Magn.* **2004**, *40*, 2988; b) A. Hultgren, M. Tanase, C. S. Chen, G. J. Meyer, D. H. Reich, *J. Appl. Phys.* **2003**, *93*, 7554.

[7] J. Kneipp, H. Kneipp, M. McLaughlin, D. Brown, K. Kneipp, *Nano Lett.* **2006**, *6*, 2225.

[8] a) G. Das, F. Mecarini, F. Gentile, F. De Angelis, H. G. M. Kumar, P. Candeloro, C. Liberale, G. Cuda, E. Di Fabrizio, *Biosens. Bioelectron.* **2009**, *24*, 1693; b) Y. Jiao, J. D. Ryckman, P. N. Ciesielski, C. A. Escobar, G. K. Jennings, S. M. Weiss, *Nanotechnology* **2011**, *22*; c) J. M. Oran, R. J. Hinde, N. Abu Hatab, S. T. Retterer, M. J. Sepaniak, *J. Raman Spectrosc.* **2008**, *39*, 1811; d) M. L. Coluccio, G. Das, F. Mecarini, F. Gentile, A. Pujia, L. Bava, R. Tallerico, P. Candeloro, C. Liberale, F. De Angelis, E. Di Fabrizio, *Microelectron. Eng.* **2009**, *86*, 1085.

[9] a) S. H. Lee, F. Q. Zhu, C. L. Chien, N. Markovic, *Phys. Rev. B* **2008**, 77; b) M. Chen, C. L. Chien, P. C. Searson, *Chem. Mater.* **2006**, *18*, 1595; c) C. L. Chien, F. Q. Zhu, J. G. Zhu, *Phys. Today* **2007**, *60*, 40.

[10] a) Y. F Zhu, J. L. Shi, W. H. Shen, X. P. Dong, J. W. Feng, M. L. Ruan, Y. S. Li, *Angew. Chem. Int. Ed.* **2005**, *44*, 5083; b) D. K. Yi, S. T. Selvan, S. S. Lee, G. C. Papaefthymiou, D. Kundaliya, J. Y. Ying, *J. Am. Chem. Soc.* **2005**, *127*, 4990; c) C. Graf, D. L. J. Vossen, A. Imhof, A. van Blaaderen, *Langmuir* **2003**, *19*, 6693.

[11] X. Xu, K. Kim, H. Li, D. L. Fan, *Adv. Mater.* **2012**, *24*, 5457.

[12] B. K. Park, S. Jeong, D. Kim, J. Moon, S. Lim, J. S. Kim, *J. Colloid Interface Sci.* **2007**, *311*, 417.

[13] a) S. M. Nie, S. R. Emery, *Science* **1997**, *275*, 1102; b) K. Kneipp, Y. Wang, H. Kneipp, L. T. Perelman, I. Itzkan, R. Dasari, M. S. Feld, *Phys. Rev. Lett.* **1997**, *78*, 1667; c) M. G. Albrecht, J. A. Creighton, *J. Am. Chem. Soc.* **1977**, *99*, 5215; d) A. Campion, P. Kambhampati, *Chem. Soc. Rev.* **1998**, *27*, 241.

[14] a) E. C. Le Ru, E. Blackie, M. Meyer, P. G. Etchegoin, *J. Phys. Chem. C* **2007**, *111*, 13794; b) F. S. Ou, M. Hu, I. Naumov, A. Kim, W. Wu, A. M. Bratkovsky, X. Li, R. S. Williams, Z. Li, *Nano Lett.* **2011**, *11*, 2538; c) M. Hu, F. S. Ou, W. Wu, I. Naumov, X. Li, A. M. Bratkovsky, R. S. Williams, Z. Li, *J. Am. Chem. Soc.* **2010**, *132*, 12820; d) M. S. Schmidt, J. Hübner, A. Boisen, *Adv. Mater.* **2012**, *24*, OP11.

[15] a) D. K. Lim, K. S. Jeon, J. H. Hwang, H. Kim, S. Kwon, Y. D. Suh, J. M. Nam, *Nat. Nanotechnol.* **2011**, *6*, 452; b) J. P. Camden, J. A. Dieringer, Y. Wang, D. J. Masiello, L. D. Marks, G. C. Schatz, R. P. Van Duyne, *J. Am. Chem. Soc.* **2008**, *130*, 12616.

[16] S. Link, M. A. El-Sayed, *J. Phys. Chem. B* **1999**, *103*, 4212.

[17] L. Gunnarsson, E. J. Bjerneld, H. Xu, S. Petronis, B. Kasemo, M. Käll, *Appl. Phys. Lett.* **2001**, *78*, 802.

[18] Q. H. Wei, K. H. Su, S. Durant, X. Zhang, *Nano Lett.* **2004**, *4*, 1067.

[19] R. Böhme, M. Richter, D. Cialla, P. Rösch, V. Deckert, J. Popp, *J. Raman Spectrosc.* **2009**, *40*, 1452.

[20] J. Kneipp, B. Wittig, H. Bohr, K. Kneipp, *Theor. Chem. Acc.* **2010**, *125*, 319.

[21] a) D. Fan, F. Zhu, R. Cammarata, C. Chien, *Phys. Rev. Lett.* **2005**, *94*; b) L. D. Qin, S. Park, L. Huang, C. A. Mirkin, *Science* **2005**, *309*, 113; c) M. J. Banholzer, L. D. Qin, J. E. Millstone, K. D. Osberg, C. A. Mirkin, *Nat. Protocols* **2009**, *4*, 838; d) M. J. Banholzer, J. E. Millstone, L. Qin, C. A. Mirkin, *Chem. Soc. Rev.* **2008**, *37*, 885; e) D. L. Fan, F. Q. Zhu, X. Xu, R. C. Cammarata, C. L. Chien, *Proc. Natl. Acad. Sci. USA* **2012**, *109*, 9309.

[22] D. L. Fan, F. Q. Zhu, R. C. Cammarata, C. L. Chien, *Nano Today* **2011**, *6*, 339.